

Acceleration of skeletal age MR examination using compressed sensing

Abstract

Purpose: Skeletal age assessment using MRI sometimes suffers from motion artifacts because of the long scan time in children. Reducing image acquisition time may provide benefits by reducing motion artifacts, increasing efficiency of examination, and creating a stress-free environment. In this article, the feasibility of accelerating MR image acquisition for children using compressed sensing (CS) was examined.

Materials and Methods: Undersampling patterns for CS were optimized and CS-based examination with the acceleration factors of 3 (CS3, 55 seconds per scan) and 4 (CS4, 41 seconds per scan) was performed for 59 subjects (35 boys and 24 girls; mean age, 9.1 years; age range, 4.4–15.3 years) using a 0.3 T scanner. The skeletal age was assessed by two raters (A and B).

Results: The interrater and intrarater reproducibility in skeletal age assessment was high (Pearson's $r = 0.966$ [CS3(A1) vs CS3(A2)], 0.962 [CS4(A1) vs CS4(A2)], 0.935 [CS3(A1) vs CS3(B)], and 0.964 [CS4(A1) vs CS4(B)]; $P < 0.001$). The errors in skeletal age assessed on the basis of CS-reconstructed images were similar to those assessed on the basis of fully Nyquist-sampled images.

Conclusion: These results demonstrate the validity and reliability of skeletal age examination accelerated by CS-MRI. We conclude that the acceleration factor of 3 was optimal.

Keywords: compressed sensing, open compact MRI, skeletal age assessment, pediatrics

Introduction

Skeletal age is a maturity indicator of children's growth and is important when diagnosing endocrine or chronic diseases, for hormonal therapy follow-up, or when predicting height for prognostic and therapeutic purposes (1). A critical literature review concluded that there is no standard method for bone age assessment (2). A radiograph of the left hand and wrist is the most commonly used and extensively developed method for examining skeletal age (3–5), but the use of magnetic resonance imaging (MRI) (6–8) has attracted attention because of its radiation-free nature and high image contrast resolution.

MR examination of children often requires sedation or anesthesia because they may not lie still for long enough in the noisy and claustrophobic environment. An open compact scanner offers a comfortable environment for children, and we have verified the validity and reliability of skeletal age assessment over a wide range of ages using this type of scanner as used in previous studies (9,10). However, motion artifacts remain an unsolved challenge in examining skeletal age with MRI. In a previous study with 2 min 44 s scan time (9), four of 93 cases were excluded from rating because of severe motion artifacts. One solution for reducing motion artifacts is to shorten the scan time. A short scan time offers the additional benefits of greater comfort for children and improved efficiency of the examination.

In this study, to provide a method for reducing the scan time of a skeletal age examination, we integrated a compressed sensing (CS) technique (11–13) using a 0.3 T open

compact scanner. We optimized the sampling pattern using knowledge of the nature of the data to be reconstructed. The purpose of this study was to investigate the feasibility and reliability of the CS-based examination of hand MRI in children.

Materials and Methods

Optimization of CS sampling pattern

First, the sampling pattern for CS was optimized using 88 images of hands obtained in the previous study (10). We chose one subset that showed high quality images and used them for optimization for 12 sets of data: 6 boys (aged 5.7, 6.5, 9.0, 10.9, 13.7, and 14.8 years) and 6 girls (aged 5.3, 7.1, 9.6, 10.5, 13.4, and 15.7 years). The optimized patterns were validated using all of the dataset. The original matrix size of the fully Nyquist-sampled (FS) image was $512 \times 128 \times 32$. Given acceleration factor R (2, 3, and 4), the undersampling pattern in the k-space was determined as a combination of the low-resolution pattern ($N_x \times N_y$ dense pattern near the center) and the sparse pattern in two phase-encoded directions with variable density.

The probability density function ρ was given by

$$\rho = A \exp \left[-\frac{k_x^2 + k_y^2}{2\sigma_x^2 + 2\sigma_y^2} \right],$$

where k_x and k_y are the coordinates in the phase direction. In the CS simulation, R was chosen to be 2, 3, and 4, and the corresponding CS reconstruction images were defined as CS2, CS3, and CS4, respectively.

In the optimization process, we prepared a total of 256 parameter sets, in which N_x and N_y varied between 8 and 32 in 8 increments, and σ_x and σ_y varied between 0.5 and 2 in 0.5 increments. Five sampling patterns were randomly generated for each parameter set. The training dataset was then undersampled according to the generated sampling pattern and reconstructed using a CS reconstruction algorithm with the fast composite splitting algorithm (FCSA) (14). In FCSA, the CS reconstructed image $\hat{\mathbf{x}}$ was obtained by having both a wavelet transform and a discrete gradient in the objective, which is formulated as follows:

$$\hat{\mathbf{x}} = \arg \min_{\mathbf{x}} \left\{ \frac{1}{2} \|R\mathbf{x} - b\|^2 + \alpha \|\mathbf{x}\|_{TV} + \beta \|\Psi\mathbf{x}\|_1 \right\},$$

where \mathbf{x} is an MR image, α and β are two positive parameters, b is the undersampled measurements of k-space data, R is a partial Fourier transform, and Ψ is a wavelet transform. Here we set $\alpha = 0.0002$ and $\beta = 0.001$, and the resultant quality of the CS images did not change significantly as these values changed. The iterative shrinkage-thresholding method (14) was used to solve the minimization problem, and the number of iterations was 50.

We calculated the structural similarity (SSIM) (15) between the FS and CS images, which is given by

$$\text{SSIM} = \frac{(2\mu_x\mu_y + c_1)(2\sigma_{xy} + c_2)}{(\mu_x^2 + \mu_y^2 + c_1)(\sigma_x^2 + \sigma_y^2 + c_2)},$$

where μ_x and σ_x are the average and variance of the FS image, μ_y and σ_y are the average and variance of the CS image, respectively, and σ_{xy} is the covariance of the FS and CS images.

Constants c_1 and c_2 are included to avoid instability when $\mu_x^2 + \mu_y^2$ is close to zero, and we

specifically chose that $c_1 = c_2 = 400$. Finally, the sampling pattern with the highest mean SSIM over the training set was chosen as the optimal pattern.

Subjects

A total of 59 healthy Japanese children (35 boys and 24 girls; mean age, 9.1 years; age range, 4.4–15.3 years) were recruited from the local community. Those with a history of genetic, developmental, metabolic, or endocrine diseases, wrist trauma, or taking medication including hormonal supplements were excluded. Written informed consent was obtained from both the children and one of their parents. All of the MRI measurements were performed with the approval of the ethics committee of the Graduate School of Pure and Applied Science, University of Tsukuba.

MR measurements

We used an open compact MRI with a permanent magnet (field strength = 0.3 T; gap = 12 cm; homogeneity = 16 ppm over a $12 \times 16 \times 8$ cm³ diameter ellipsoidal volume; weight = 450 kg; Shine-etsu, Chemical Co. Ltd., Tokyo, Japan), which was developed for skeletal age examination in children (10). The radiofrequency (RF) coil was a 16-turn, 17.6-cm-long solenoid. The RF coil was shielded by a rectangular RF probe box made of brass plates. A 5-mm-thick aluminum plate was connected to the outside of the shield box to ground the arm and

thus minimize interference by external RF noise. To reduce motion, each subject sat in a chair and watched a television screen with his or her hand loosely fixed onto a plastic plate by a flexible cloth belt.

A three-dimensional (3D) coherent gradient-echo sequence (dwell time = 20 μ s; TR/TE = 40/11 ms; flip angle = 60°; matrix size = 128 \times 512 \times 32; field of view (FOV) = 10 cm \times 20 cm \times 5 cm, acquisition time for FS imaging = 2 min 44 s) was used. Three image sets were obtained for the distal and proximal parts: the normally reconstructed image with the full sampling pattern (FS, $R = 1$), and the CS-reconstructed images with the optimal sampling patterns of $R = 3$ (CS3, acquisition time = 55 s) and $R = 4$ (CS4, acquisition time = 41 s).

MRI skeletal rating

Skeletal age was rated independently by two raters. Rater A (RM) has 11 years of experience as an orthopedic surgeon and 5 years of experience in rating skeletal age using MRI; rater B (TN) has 13 years of experience in musculoskeletal radiology and 3 years of experience in rating skeletal age using MRI. The raters were blinded to the children's age. The MR images were sorted in a random order irrespective of the CS acceleration factors, and the raters performed independent blinded assessments of different acceleration factors. The children's ages were scored according to the Tanner–Whitehouse Japan RUS system (RUS stands for

radius, ulna, and the 11 short bones in rays 1, 3, and 5) (16). Rater A rated twice (A1 and A2) after a 2-week interval to investigate the intrarater reproducibility.

Image evaluation

The denoising process in the CS reconstruction may alter the noise level in the images. To address this, the signal-to-noise ratio (SNR) was calculated for the metacarpal in ray 3 in the distal-part image and for the radius in the proximal-part image.

The randomized MR images were assessed independently for overall image quality and artifacts such as motion, low SNR, and being out of the FOV by the two raters. The overall image quality was graded on a 4-point scale: 1 = nondiagnostic, 2 = fair, 3 = good, and 4 = excellent. Each artifact was graded on a 2-point scale: 0 = image without artifact and 1 = image with artifact.

Statistical analysis

Simple linear regression analysis was used to determine the correlation between chronological age and MRI skeletal age. To measure interrater (A1 vs B and A2 vs B) and intrarater (A1 vs A2) reproducibility, Pearson's correlation coefficient (r) and mean absolute errors between the skeletal ages assessed on the basis of the FS, CS3, and CS4 images were calculated. The values of Cohen's weighted κ (17) were calculated to evaluate the agreement

between ratings for individual RUS bones separately. According to the guideline for strength of agreement (17), κ values of 0.41–0.60, 0.61–0.80, and 0.81–1.0 were considered to indicate moderate, substantial, and almost perfect agreement, respectively. A two-tailed paired Wilcoxon rank test was used to identify significant differences between the different acceleration factors with respect to the appearance of various image artifacts. A P -value <0.05 was considered significant.

Results

Validation of CS sampling pattern

The optimal patterns were validated with the whole dataset (Fig. 1). The mean SSIMs were 0.89 (CS2), 0.79 (CS3), and 0.72 (CS4) for the distal parts, and 0.93 (CS2), 0.86 (CS3), and 0.80 (CS4) for the proximal parts. The SSIM was nearly independent of the chronological age. In most cases of CS2 and CS3, the SSIM values were >0.75 which was considered to be an acceptable value for similarity assessment in this study (see Supporting information for the derivation of the acceptable value). For CS4, the SSIM values were mostly above the acceptable value for the proximal parts, but not for the distal parts.

MR images

Figure 2 shows an example of the reconstruction with the full data (FS) and the CS reconstruction with $R = 3$ and 4 (CS3 and CS4). The geometric features of the RUS bones were distinguishable in the CS3 and CS4 images. The structural differences between the epiphyses and metaphysis of the RUS bones were resolved clearly. The SNRs in the distal (28.3 [FS], 25.9 [CS3] and 28.5 [CS4]) and proximal (30.4 [FS], 33.3 [CS3], and 33.9 [CS4]) parts were almost the same. Figure 3 shows an example of MR images with motion, low SNR, and out-of-FOV artifacts as assessed by the raters.

Reliability of rating

The correlation coefficients for the repeated measurements of skeletal age rated by rater A at different times were high ($r = 0.959$ (A1 vs A2 for FS), 0.966 (A1 vs A2 for CS3), and 0.962 (A1 vs A2 for CS4), indicating high intrarater reproducibility. The correlations between the skeletal ages rated by raters A and B were also high ($r = 0.948$ (A1 vs B for FS), 0.935 (A1 vs B for CS3), 0.964 (A1 vs B for CS4), 0.927 (A2 vs B for FS), 0.956 (A2 vs B for CS3), and 0.940 (A2 vs B for CS4)), indicating high interrater reproducibility. In all of these cases, the P-values for the correlation coefficients were <0.001 .

Comparison of skeletal age assessment on the basis of FS and CS images

Figure 4 shows a comparison between skeletal ages assessed on the basis of the FS and CS-reconstructed images. Table 1 shows Pearson's correlation coefficients and mean absolute errors between the skeletal ages assessed on the basis of the FS, CS3, and CS4 images. All of the correlation coefficients were >0.9 ($P < 0.001$), and most of the mean absolute errors were <1.0 year. The errors between FS and CS3, and those between FS and CS4, were similar to the errors between FS(A1) and FS(A2).

Table 2 shows the Cohen's weighted κ calculated for the rated scores of each bone. In most cases, the average κ was >0.80 , which indicates nearly perfect agreement. Individual bones also showed high κ values >0.60 , indicating substantial agreement.

Image quality and failure of assessment

Figure 5(a) shows the overall image quality evaluated by the two raters. The numbers of images with good or excellent quality were large for FS, CS3, and CS4. There were no significant differences in the overall image quality between FS, CS3, and CS4 ($P > 0.01$).

Figure 5(b) and 5(c) show the number of image artifacts. Both raters assessed that motion artifacts appeared less frequently for CS3 than for FS. For rater A, the difference between FS and CS3 with respect to motion appearance approached but did not reach statistical significance ($P = 0.11$). For rater B, the difference was significant ($P < 0.05$). The motion differences between FS and CS4 were not significant for the two raters, and those between CS3

and CS4 were not significant for rater A ($P = 0.34$) but were significant for rater B ($P < 0.01$).

The numbers of motion artifacts for children aged <10 years were 14 (FS), 9 (CS3), and 9 (CS4) for rater A, and 16 (FS), 8 (CS3), and 15 (CS4) for rater B.

The numbers of low SNR artifacts were largest for CS4, although the differences between FS, CS3, and CS4 were not significant with the exception that the difference between CS3 and CS4 was significant for rater B. The total numbers of artifacts were largest for CS4. For rater A, the difference between FS and CS4 was significant ($P < 0.01$). For rater B, the differences between FS and CS3, and between CS3 and CS4, were significant ($P < 0.01$).

Discussion

There are several methods for reducing scan time. Partial-Fourier acquisition is a traditional, simple method, but the acceleration factor ranges from 1.3 to 1.8 in most cases (18). The use of radial or spiral trajectory with reduced sampling points may be another solution, but this has certain limitations such as a high sensitivity to field inhomogeneity, thermal drift, and eddy current field (19). Parallel imaging with multiple receiver coils is also a technique for shortening the scan time by reducing the dataset in the phase-encoding direction of the k-space and is now widely used in clinical settings (20). CS is a promising technique that accelerates MR image acquisition in different applications (12,21,22). Although the advantages of CS

acceleration are obvious, there is only limited experience in using CS-reconstructed images in preclinical or clinical routines (23).

We have described a method for accelerating skeletal age measurement using CS. The key components of CS are the random incoherent undersampling to avoid coherent artifacts and nonlinear reconstruction to recover the sparse signal. The image quality of the CS image is determined mainly by the sparsity and incoherence of the signal (24,25), and the CS-reconstruction method and parameters have less importance in the resultant image. Making the appropriate choices for a given application is important for obtaining high reconstruction performance. Accordingly, we optimized the undersampling patterns in the k-space trajectory using a data-driven framework. Although only parts of the datasets were used for optimization to reduce the computational burden, the optimized trajectories yielded high SSIM values for all datasets. The SSIM values were nearly independent of chronological age, and this should ensure that the optimized patterns are applicable to all age groups.

We have examined the validity of the CS-accelerated examination experimentally, and we have proven that the method provides images that are similar to noncompressed images for the following reasons. First, the skeletal ages assessed on the basis of the CS and FS images were in good agreement with each other. They showed high correlations, and the errors in the skeletal age rated from the FS and CS images were similar to the intrarater and interrater errors in the FS-based ratings. Second, agreement was high for the rated score for each bone, even

for the small, short bones. Third, the raters assigned mostly high (good or excellent) quality scores to the CS3 and CS4 images, which were comparable to the FS images.

Motion artifacts appeared less frequently for CS3 than for FS, probably because of the reduced scan time, although the difference did not reach statistical significance for rater A. This is partly because the probability of motion appearance was low and the number of examinations in this study was too small to detect a difference. The number of motion artifacts was not small for CS4 although its scan time was the shortest. This is presumably because the examinations of FS, CS3, and CS4 were performed in this order without a break, and the children might have been exhausted by having to remain still at the time of the CS4 scan. Despite these facts, it is obvious that reducing examination time has a clinical benefit for reducing motion. There may be cases where hand motion occurs intermittently but not continuously. Some children may keep still at the beginning of the examination but may tire gradually as the examination time passes. In such cases, the reduced examination time would increase the chance of finishing the examination before the child tires and moves the hand, and this would reduce the possibility of motion appearance. In a clinical setting, if the assessment cannot be completed because of motion artifacts, it is necessary to repeat the examinations. If the examination time can be shortened by using CS, re-examination is also more likely to be successful.

There were few significant differences in the artifact appearance in the low SNR and out-of-FOV images. The total number of artifact appearances was significantly larger for CS4

compared with CS3 and FS. Thus, the examination using the CS4 protocol may be difficult for raters to score and may therefore increase the likelihood of errors, especially with a large number of subjects. For these reasons, we conclude that the CS3 protocol was optimal for our study.

Our study has several limitations. First, we have no reference standard against which to confirm bone age. Bone age assessment by the Tanner–Whitehouse Japan RUS system is based on radiography of the hand. However, exposure of healthy volunteers to plain radiography cannot be justified. Our application of the Tanner–Whitehouse Japan RUS system for bone age assessment by MRI has been used in a previous study (9). Second, we did not compare the image quality between CS-MRI and other reduced scan techniques such as half-Fourier acquisition or parallel imaging techniques with multiple receiver coils. Third, we included only a limited number of subjects, and further studies with more subjects are needed to confirm our results. Fourth, it is unclear whether CS delivers sufficiently consistent image quality in skeletal age assessment for routine clinical use. This issue could be clarified by a comparative study using X-ray examination. Fifth, the measurements with different acceleration factors were performed in a single session, which may have led to bias in the occurrence of motion artifacts. To detect a possible effect of reduced examination times on motion artifacts, the measurements should be performed in a random order.

In this study, healthy volunteers were examined. However, for many applications, the results are worse for MR imaging of patient compared with healthy volunteers. It would thus be of interest to examine the results of the proposed methods in a clinical setting.

Conclusion

We integrated the CS technique into skeletal age examination and examined the validity of our method. The undersampling patterns were optimized using the database of hand images at a given R . The acquisition time for CS-based examination was reduced to be within 1 min (55 s for $R = 3$ and 41 s for $R = 4$). The feasibility and reliability of the CS-based skeletal examination was demonstrated experimentally. We conclude that the acceleration factor of 3 was optimal. The accelerated skeletal age examination using CS-MRI may be clinically useful.

References

1. Bertaina C, Stasiowska B, Benso A, Vannelli S. Is TW3 height prediction more accurate than TW2? Preliminary data. *Horm Res* 2007;67:220-223.
2. Mughal AM, Hassan N, Ahmed A. Bone age assessment methods: A critical review. *Park J Med Sci* 2014;30:211-215.
3. Acheson RM. A method of assessing skeletal maturity from radiographs; a report from the Oxford child health survey. *J Anat* 1954;88:498-508.
4. Greulich WW, Pyle SI. Radiographic atlas of skeletal development of the hand and wrist. 2nd ed. Stanford, Calif.,: Stanford University Press; 1959.
5. Tanner JM. Assessment of skeletal maturity and prediction of adult height (TW2 method). 2nd ed. London; New York: Academic Press; 1983.
6. Dvorak J, George J, Junge A, Hodler J. Age determination by magnetic resonance imaging of the wrist in adolescent male football players. *Br J Sports Med* 2007;41:45-52.
7. George J, Nagendran J, Azmi K. Comparison study of growth plate fusion using MRI versus plain radiographs as used in age determination for exclusion of overaged football players. *Br J Sports Med* 2012;46:273-278.

8. Dvorak J, George J, Junge A, Hodler J. Application of MRI of the wrist for age determination in international U-17 soccer competitions. *Br J Sports Med* 2007;41:497-500.
9. Terada Y, Kono S, Tamada D, Uchiumi T, Kose K, Miyagi R, Yamabe E, Yoshioka H. Skeletal age assessment in children using an open compact MRI system. *Magn Reson Med* 2013;69:1697-1702.
10. Terada Y, Kono S, Uchiumi T, Kose K, Miyagi R, Yamabe E, Fujinaga Y, Yoshioka H. Improved reliability in skeletal age assessment using a pediatric hand MR scanner with a 0.3T permanent magnet. *Magn Reson Med Sci* 2014;13:215-219.
11. Donoho D. L. Compressed sensing. *IEEE Trans Inf Theory* 2006;52:1289-1306.
12. Lustig M, Donoho D. L., Pauly J. M. Sparse MRI: The application of compressed sensing for rapid MR imaging. *Magn. Reson. Med.* 2007;58:1182-1195.
13. Lustig M, Donoho D. L., Santos J. M., Pauly J. M. Compressed sensing MRI. *IEEE Signal Processing Magazine* 2008;25:72-82.
14. Huang J, Zhang S, Metaxas D. Efficient MR image reconstruction for compressed MR imaging. *Med Image Analysis* 2011;15:670-679.
15. Wang Z, Bovik A C, Sheikh H R, Simoncelli E P. Image quality assessment: from error visibility to structural similarity. *IEEE Trans Image Processing* 2004;13:600-612.

16. The Japanese Society for Pediatric Endocrinology and The Japanese Association for Human Auxology ed., Assessment of skeletal age for Japanese children. Tokyo: Medical View; 2011 [in Japanese].
17. Kundel H L, Polansky M. Measurement of observer agreement. *Radiology* 2003;228:303-308.
18. Bernstein M A, King K F, Zhou X J. Handbook of MRI pulse sequences, San Diego, CA: Elsevier Academic Press; 2004. 548 p.
19. Delattre B M A, Heidemann R M, Crowe L A, Vallée J P, Hyacinthe J N. Spiral demystified. *Magn Reson Imaging* 2010;28:862-881.
20. Deshmane A, Gulani V, Griswold M A, Seiberlich N. Parallel MR imaging. *J Magn Reson Imaging* 2012;36:55-72.
21. Gamper U, Boesiger P, Kozerke S. Compressed sensing in dynamic MRI. *Magn Reson Med* 2008;59:365-373.
22. Smith DS, Li X, Abramson R G, Quarles C C, Yankeelov T E, Welch E B, Potential of compressed sensing in quantitative MR imaging of cancer. *Cancer Imaging* 2013;13:633-644.
23. Hollingsworth K G. Reducing acquisition time in clinical MRI by data undersampling and compressed sensing reconstruction. *Phy Med Biol* 2015;60:R297-322.

24. Candes E J, Tao T. Near-optimal signal recovery from random projections: universal encoding strategies? IEEE Trans Inf Theory 2006;52:5406-5425.
25. Candes E J, Wakin M B. An introduction to compressed sampling. IEEE Signal Proc Mag 2008;23:21-30.

Table 1 Comparison between FS- and CS-based ratings.

	Pearson's r	Mean absolute error [years]
FS(A1) – FS(A2) [reference]	0.959	0.70
FS(A1) – CS3(A1)	0.900	1.0
FS(A1) – CS4(A1)	0.942	0.98
FS(A2) – CS3(A2)	0.949	0.78
FS(A2) – CS4(A2)	0.952	0.86
FS(B) – CS3(B)	0.945	0.98
FS(B) – CS4(B)	0.931	1.1

P values for the correlation coefficients were <0.001 in all cases. FS(A1), FS(A2), and FS(B)

denote skeletal ages assessed by raters A (A1 and A2) and B on the basis of the fully-sampled

images. CS3(A1), CS3(A2), and CS(B) denote those on the basis of the CS3 images.

CS4(A1), CS4(A2), and CS(B) denote those on the basis of the CS4 images.

Table 2 Agreement of scoring results for different bones.

	Radius	Ulna	MC I	MC III	MC V	PP I	PP III	PP V	MP III	MP V	DP I	DP III	DP V	Average
FS(A1) vs CS3(A1)	0.74	0.90	0.84	0.75	0.77	0.87	0.77	0.80	0.66	0.78	0.77	0.75	0.85	0.79
FS(A1) vs CS4(A1)	0.77	0.94	0.82	0.76	0.83	0.77	0.67	0.77	0.77	0.76	0.84	0.77	0.82	0.79
FS(A1) vs FS(A2)	0.90	0.98	0.89	0.79	0.85	0.91	0.89	0.88	0.86	0.90	0.90	0.89	0.88	0.89
FS(A2) vs CS3(A2)	0.88	0.97	0.89	0.80	0.83	0.83	0.76	0.83	0.79	0.86	0.89	0.87	0.88	0.85
FS(A2) vs CS4(A2)	0.84	0.97	0.86	0.76	0.81	0.83	0.75	0.80	0.78	0.80	0.86	0.83	0.78	0.82
FS(A1) vs FS(A2)	0.90	0.98	0.89	0.79	0.85	0.91	0.89	0.88	0.86	0.90	0.90	0.89	0.88	0.89
FS(B) vs CS3(B)	0.80	0.93	0.88	0.83	0.83	0.88	0.81	0.88	0.82	0.82	0.87	0.90	0.89	0.86
FS(B) vs CS4(B)	0.71	0.92	0.86	0.81	0.80	0.85	0.80	0.83	0.80	0.75	0.82	0.86	0.89	0.82
FS(B) vs FS(A1)	0.73	0.92	0.91	0.83	0.83	0.85	0.77	0.82	0.76	0.81	0.88	0.84	0.84	0.83

MC, metacarpal; PP, proximal phalanx; MP, middle phalanx; DP, distal phalanx. FS(A1),

FS(A2), and FS(B) denote bone scores assessed by raters A (A1 and A2) and B on the basis

of the fully-sampled images. CS3(A1), CS3(A2), and CS(B) denote those on the basis of the

CS3 images. CS4(A1), CS4(A2), and CS(B) denote those on the basis of the CS4 images.

Figure captions

Fig. 1 Validation of optimized sampling patterns. The structural similarity (SSIM) values for (a) distal and (b) proximal part images are plotted as a function of chronological age.

Fig. 2 MR images of the left hand of a healthy 8.6-year-old girl.

Fig. 3 Example of MR images with (a) motion (4.8 years, girl), (b) low SNR (9.1 years, girl), and (c) out-of-FOV (9.9 years, girl).

Fig. 4 Agreement of skeletal age assessed on the basis of FS images and CS-reconstructed images (CS3 and CS4). (a) Intrarater agreement. (b) and (c) Interrater agreement.

Fig. 5 Evaluation by raters. (a) Image quality evaluation. (b) and (c) Numbers of cases in which a certain artifact appeared, as reviewed by (b) rater A and (c) rater B. The total number corresponds to the number of cases where any motion, low SNR, or out-of-FOV artifacts appeared. * $P < 0.05$; ** $P < 0.01$.

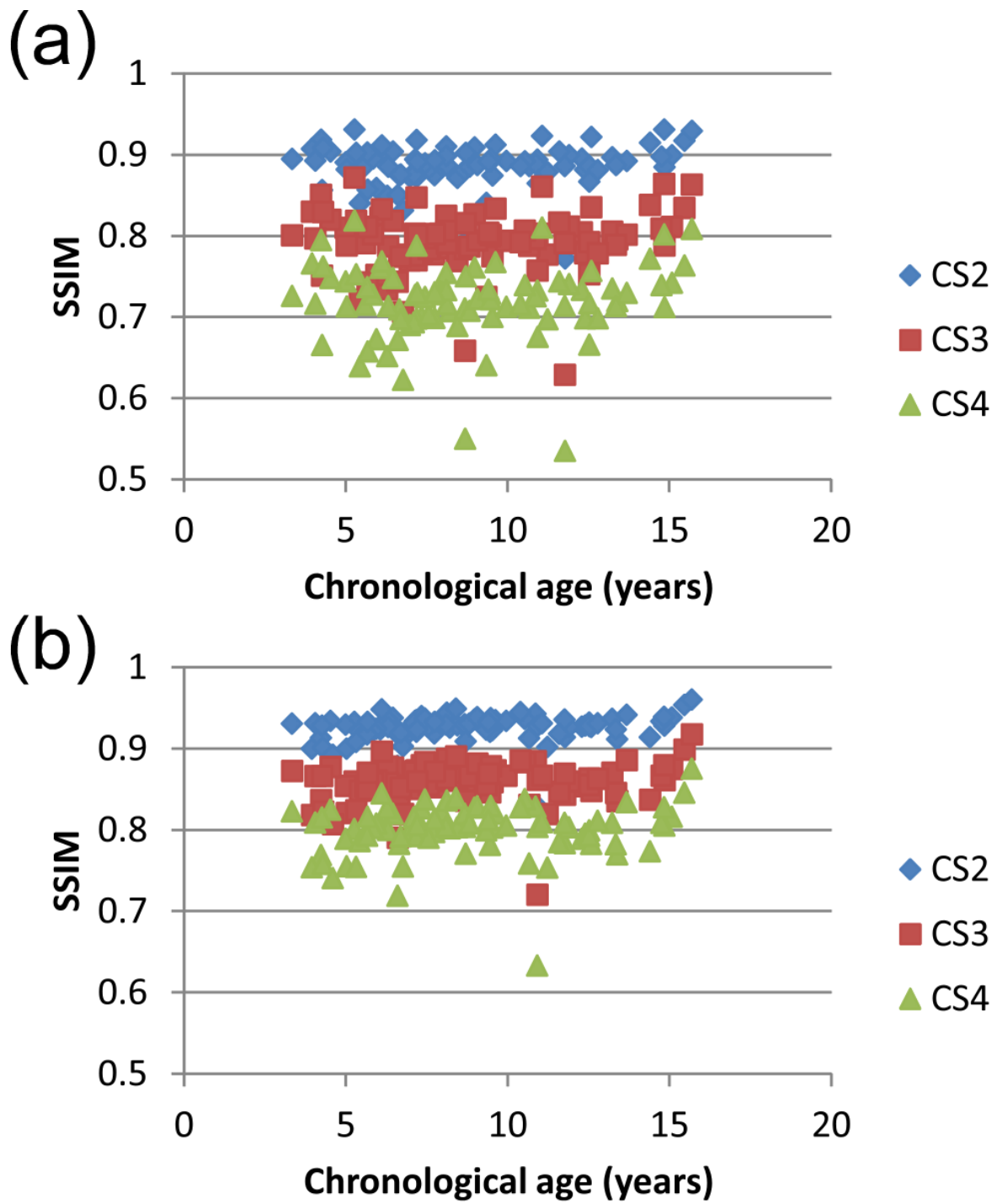
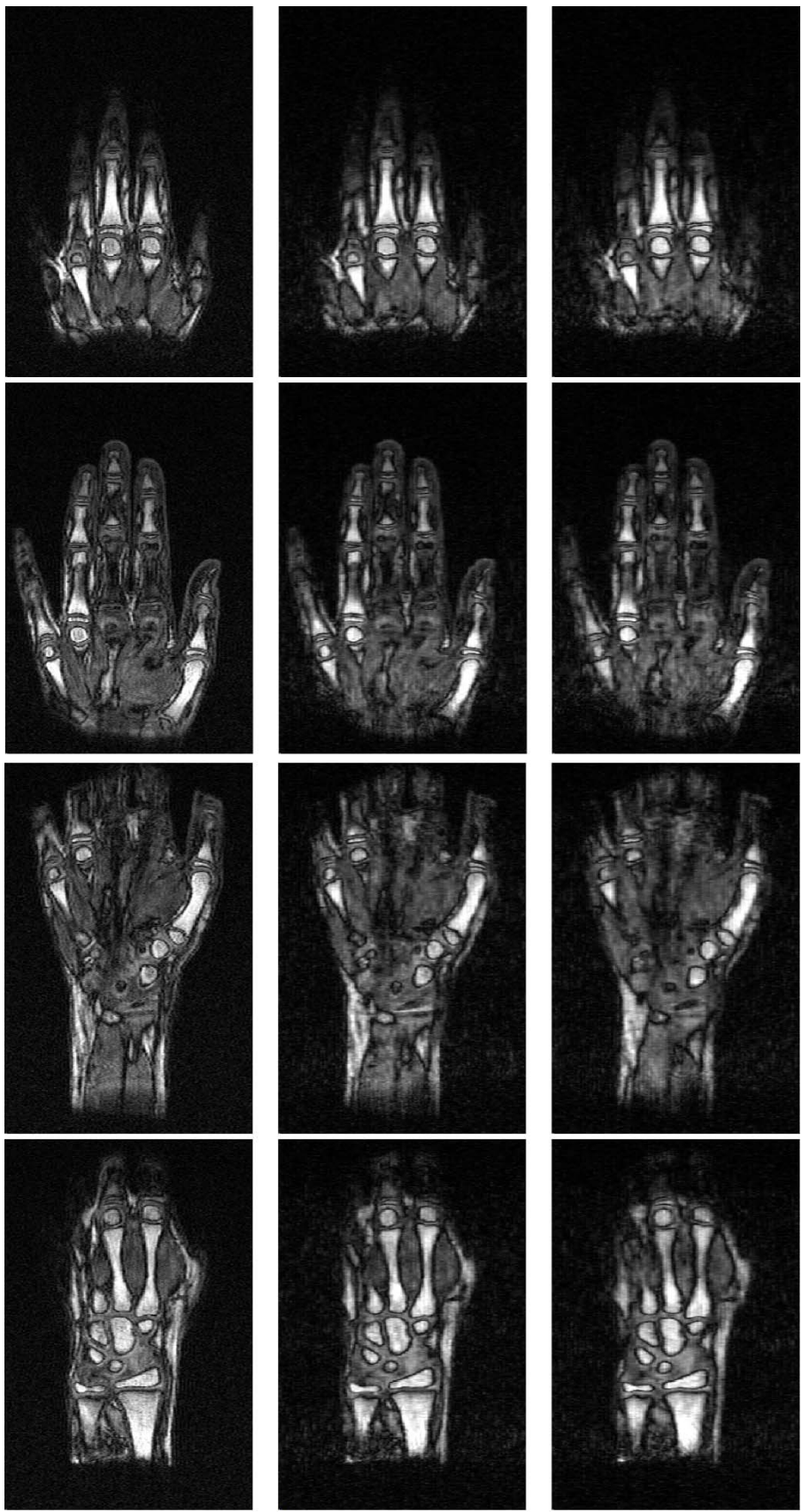


Fig. 1



FS, 2 min 44 s

CS3, 55 s

CS4, 41 s

Fig. 2

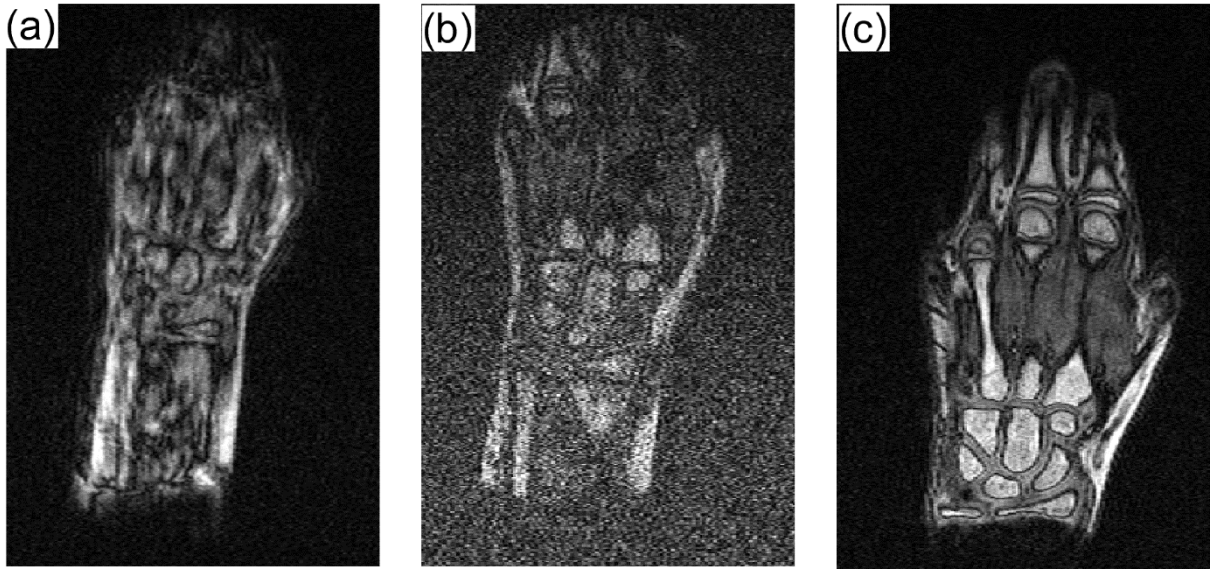


Fig. 3

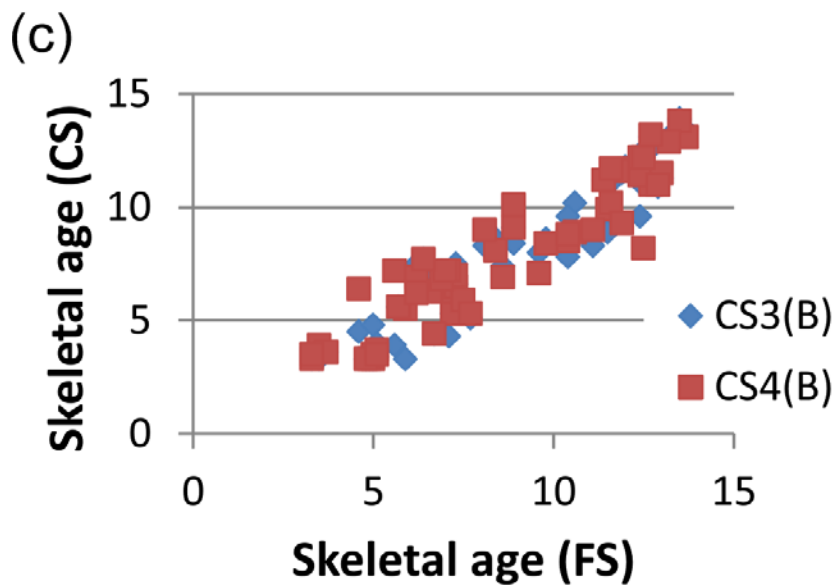
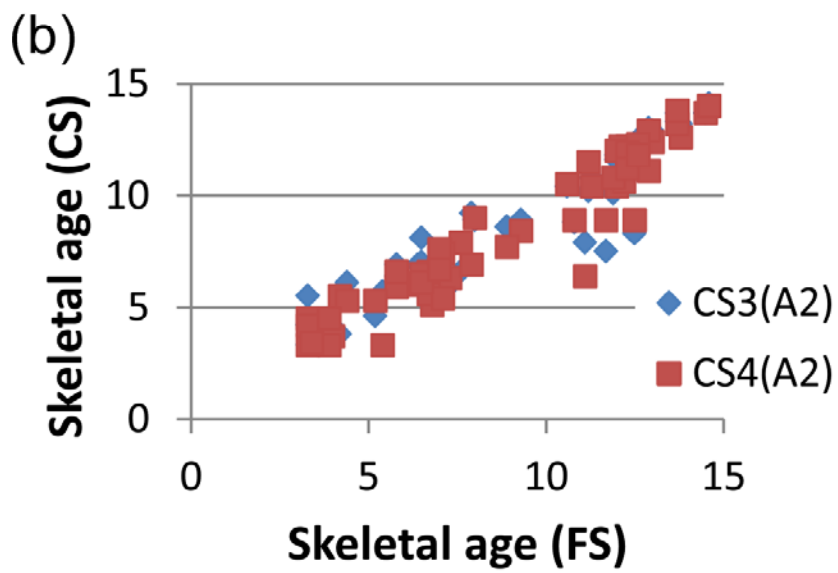
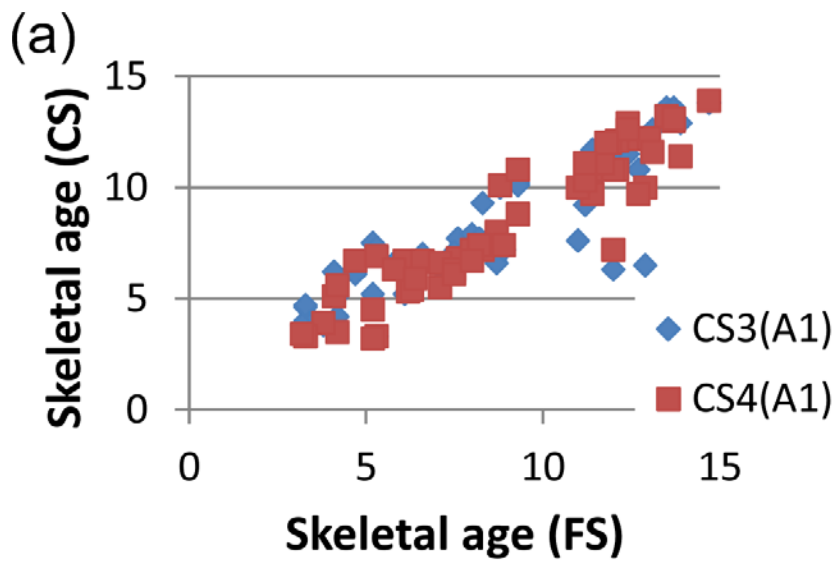


Fig. 4

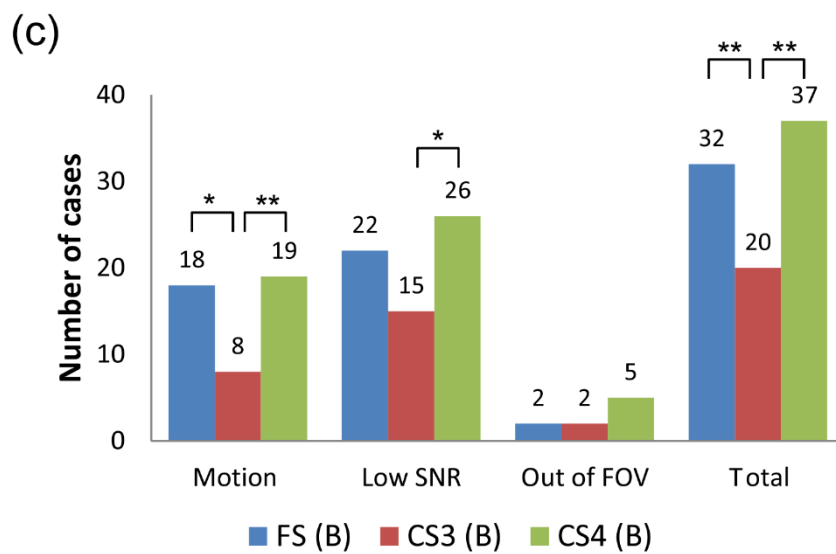
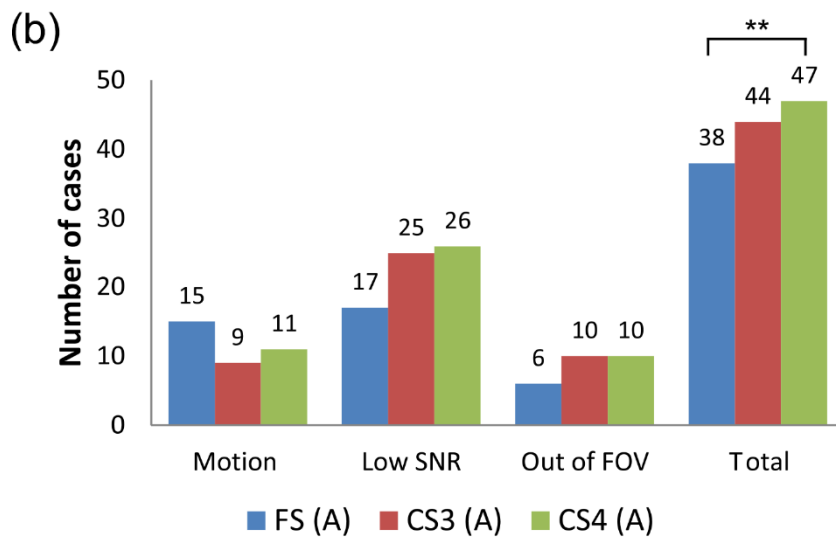
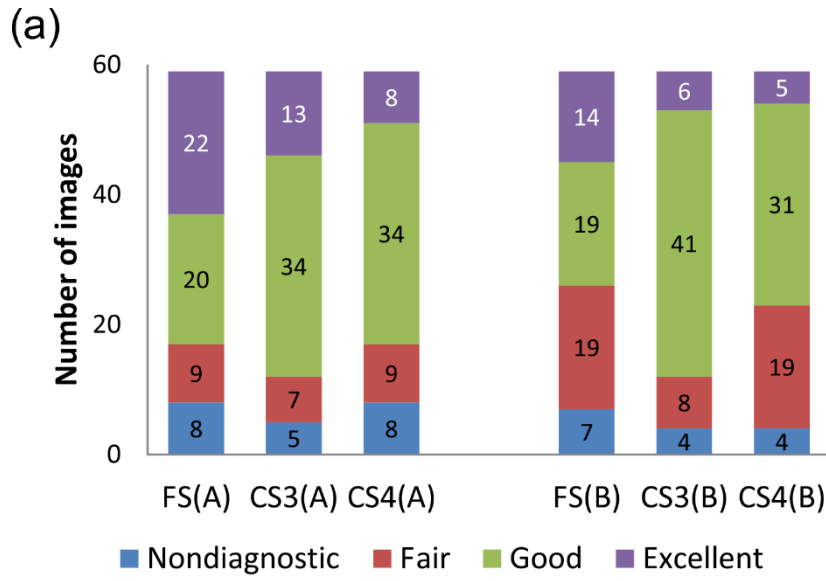


Fig. 5